Accessibility Framework for Determining Collisions and Coverage for Radiation Scanning.

Joshua Bettles[1 [0000−0002−1193−252X]], Andrew West[1 [0000−0003−4553−8640]], Jeremy Andrew[2 [0009−0009−9352−8181]], Iain Darby[3,4 [0000−0003−2091−2616]], and Barry Lennox[1 [0000−0003−0905−8324]]

[1] Manchester Centre for Robotics and AI, The University of Manchester, Manchester, M13 9PL, UK
joshua.bettles@manchester.ac.uk
[2] Nuclear Restoration Services Ltd. Dounreay, Thurso, Caithness, KW14 7TZ, UK
[3] National Nuclear Laboratory, Chadwick House, Birchwood Park, Warrington, Cheshire, WA3 6AE, UK
[4] School of Physics and Astronomy, University of Glasgow, Glasgow, G12 8QQ, U.K

Abstract. Radioactive contamination monitoring is an important part of radiological protection. Automation of surface monitoring poses difficulties, with a major challenge being determining the coverage of a radiation probe over an object in close proximity without collision. We propose a new accessibility framework to determine if radiation probes, modelled as convex hulls, collide with 3D point clouds representing the objects. We explain how to structure and analyze point clouds to extract properties such as the surface normal for each point. Our method for approximating radiation probes is demonstrated using the BP4 probe. This approach models both the probe and the sensor's effective scan volume with geometric primitives, providing a computationally efficient way to detect collisions with flat surfaces. The accessibility assessment builds on common methods within computer science for determining intersections. A laptop in various positions was used to demonstrate that the framework can efficiently categorise points as accessible or inaccessible, identifying unscannable regions. The output of this framework can then be used to plan collision-free paths over objects and will be the foundation of a robotic survey assistant.

Keywords: Accessibility Assessment · Contamination Monitoring · Discrete Collision Detection · Health Physics · Point Cloud · Nuclear

1 Introduction

Within the nuclear industry, many roles involve possible contact with radioactive materials, from laboratory experimentation to decommissioning work; these activities take place in controlled or supervised areas. The scientists and engineers who work in these areas require the use of Personal Protective Equipment (PPE). This PPE protects individuals and reduces the possibility of spreading contamination from high-level controlled zones to lower zones. To limit the spread of

contamination, the removal of PPE must be carried out in buffer zones and at barriers between controlled areas. All sites have contamination monitoring equipment and health physics specialists situated at each egress point between buffer zones, barriers and controlled areas to perform examinations of individuals to ensure that no residual contamination is present [9]. Several reports [1,14] have highlighted the declining availability of the radiological protection workforce. Robotics could alleviate the demand for roles such as health physics specialists by automating these mundane tasks.

Small and large article transfer monitors [4] and full body contamination monitors [18] are frequently used for contamination monitoring at these barriers but are limited in their application. Many systems are single purpose, i.e. only used for scanning humans or objects of a certain size, and for use detecting β/γ contamination due to the short mean free path of α. Automation of contamination monitoring poses a challenging application for robotics. For example, robotic manipulators equipped with radiation probes could perform autonomous monitoring operations, and advances in perception and control could allow for the system to be used on any object, material, or personnel presented.

Radioactive contamination monitoring using robotics is a multi-faceted problem which is a growing field in the literature. Recent work by White *et al.* [21] used an industrial robotic manipulator to map and profile radioactive sources on a flat surface. Whilst work by Mauer and Kawa [8] used a manipulator and forklift to characterise large building surfaces, performing at a distance of 1 cm whilst avoiding unknown obstacles. These systems are limited by their application, with [8] constrained to flat surfaces and paths. Monk *et al.* developed a low-cost system which was able to scan over the tops of objects and identify source locations, this was able to perform over various shaped objects however only performed these tasks in a line, not completely covering the object [10]. The work presented differs from the previous approaches as it aims to be used over complex geometries, where accessibility is considered to maximise coverage by a given probe. It will be tested on various complex geometries that will likely be found at barriers.

Contamination monitoring using manipulators is analogous to many surface following approaches. Many industries are concerned with the topic of the surface following from spray-painting, polishing, laser scanning, and more recently medical applications. Surface following can be divided into two broad categories: in-contact or at-distance. Each of these follows a similar approach of scanning the surface to create a point cloud, generating a path, and then executing a task along that path over the Volume of Interest (VoI), differing only in their control strategies, overlap, collision avoidance and stand-off distance. In-contact is common in the field of medical ultrasound, Graumann *et al.* utilised a depth camera to capture a point cloud which was used to generate trajectories over a convex hull representing the VoI [2]. A review of robotic medical ultrasound imaging and their levels of autonomy [20] concluded that there is a current limitation in robust and reliable navigation as well as the safety strategies used.

At-distance systems need to work in close proximity to the surface whilst avoiding collisions with the object. It has been demonstrated that high levels of coverage can be achieved through projecting 3D meshes created from point clouds to 2D for coverage planning [7] and was demonstrated on flat and curved surfaces. A mode-switching motion controller [12] for vehicle inspection can swap between surfaces following approaches. Obstacle avoidance was performed by moving to a safe distance away during the scan path [11]. Collision avoidance during the motion was considered. In [11] the motion did not follow the surface of the obstacle resulting in decreased coverage. This cannot occur in contamination monitoring, both works considered the size of the scanner to assess the coverage of the surfaces. However, with the complex geometries of radiation probes and the objects they will scan, the framework will place accessibility and coverage at the forefront.

Radiation scanning requires the detector to be in close proximity, 10-20 mm to the surface. Collisions are strictly prohibited as they could result in contamination or damage to the sensor, invalidating the sensor readings. Furthermore, contact with the object or personnel could spread contamination or potentially cause damage to the object or cause injury to the individual.

None of the previous work looked at the geometry of the tools and their accessibility to cover areas of a surface. This framework aims to fill this gap by considering the geometry of the probes and the effective scan volumes to determine the accessibility and coverage of objects whilst ensuring no collisions. The framework is able to analyse and identify areas of residual contamination which would require further examination.

Automating the monitoring process can be broken down into 3 stages: Data Processing, Motion Planning and Control, and Human Robot Interaction (HRI). The focus of this paper will be to develop the data processing framework. The main contribution of this paper is a new framework which:

- Enables modelling of the radiation probe and effective scan volume.
- Expands on current discrete collision detection approaches with application specific parameters.
- Determines accessibility of point clouds and regions of residual contamination.

The remainder of this paper is structured as follows. Section 2 will introduce the framework used for processing and determining the accessibility of a point cloud. The results of this approach and discussion of the outcomes will be highlighted in Section 3. Concluding remarks and future work will be discussed in Section 4.

2 Framework

This framework draws on work done by [3,16] to combine Point Cloud (PC) analysis techniques with those of spatial partitioning and normal estimation [5]. The framework extends the Discrete Collision Detection (DCD) approach [15]

and describes a method to model probe geometries and their Effective Scan Volume (ESV), that is the volume of space in front of the probe in which it can detect radiation, as convex hulls. This results in a novel accessibility assessment which can identify areas of inaccessibility on a PC, subsequently highlighting areas which pose a risk of containing residual contamination.

2.1 Spacial Partitioning and Surface Normal Estimation

When working with unorganised PC data, the initial task is to spatially partition the data in such a way that it allows for efficient searching of the data. Two common approaches for spacial subdivision are k-d trees and octrees; each allows for efficient and quick searching for the Nearest Neighbours (NN) in a given region. Octrees are shallow data structures which have 8 child nodes, splitting around a point rather than an axis like k-d trees, and do not suffer from becoming unbalanced with the insertion of new data.

Octrees generate a bounding box around the point data with equal edge lengths. Each bounding box which encapsulates a series of points is known as an octant. When each of these octants exceeds the number of allowable points within (bin number), the space is subdivided into 8 child octants with edge lengths equal to half that of the parent octant. This continues recursively until either the number of points within an octant is less than or equal to the bin number or the minimum allowable edge length of the octant is reached. This allows for control over the resolution of the generated Octree.

It has been shown by [3] that utilising Principal Component Analysis (PCA), it is possible to discern certain properties of a PC given the set of NN. The set of points forming the point cloud can be described as $P = \{\mathbf{p}_1, \cdots, \mathbf{p}_K\}$, with each point representing a location in three dimensions $\mathbf{p} \in \mathbb{R}^3$, with the set of Nearest Neighbours as

$$N_i = \{\mathbf{p}_i \in P : ||\mathbf{p}_i - \mathbf{q}_j|| < r\}, \quad \forall j \in K \tag{1}$$

where $K = |P|$ is the cardinal of the point set, $\mathbf{q}_j$ is our query point and r is a specified radius. This forms a family of sets $\{N_i\}_{\mathbf{p}_i \in P}$ where each element of N_i is a set of nearest neighbours indexed by P.

From this, it is possible to build a 3×3 covariance matrix $\mathbf{\Sigma}$, $\forall \mathbf{p} \in P$ which is given by

$$\Sigma_i = \frac{1}{k} \sum_{j \in N_{\mathbf{p}_i}} (\mathbf{p}_j - \overline{\mathbf{p}_i})(\mathbf{p}_j - \overline{\mathbf{p}_i})^T \tag{2}$$

where k is the number of nearest neighbours and $\mathbf{p}_j$ is each point in $N_{\mathbf{p}_i}$, $\overline{\mathbf{p}_i}$ is the centroid calculated at $\mathbf{p}_i$ from the nearest neighbours. The eigendecomposition of this covariance matrix can be expressed as $\mathbf{\Sigma} \cdot \mathbf{X} = \lambda \cdot \mathbf{X}$, where $\mathbf{X}$ is the matrix of eigenvectors and λ is a diagonal matrix of the eigenvalues. The eigenvectors form an orthogonal frame at the point, $\overline{\mathbf{p}_i}$, with each vector corresponding to a principal component of the spread of points [16]. Given that $\lambda_3 \geq \lambda_2 \geq \lambda_1 \geq 0$

, λ_1 is the eigenvalue which corresponds to the normal and therefore the first column of the $\mathbf{X}$ matrix corresponds to the normal vector, $\mathbf{n}_i$, at the point $\mathbf{p}_i$. The estimated normals are aligned utilising a Minimum Spanning Tree (MST) as described in [5].

2.2 Modelling of A Radiation Probe and Effective Scan Volume

The nuclear industry uses radiation probes for a variety of scanning applications, one of which is radiological protection. These devices have become ingrained in the daily operation of many facilities, and a surplus of these devices typically exists. Generating Computer-Aided Design (CAD) models for these probes is time-consuming, and requires knowledge of 3D modelling software. However, most devices can be simplified and represented by a combination of geometric primitives such as planes, cones, spheres, and cylinders. Two examples of common probes are shown in Fig. 1.

Fig. 1: DP6 (left) and BP4 (right) radiation probes supplied by Thermo Fisher Scientific [19].

Consider the BP4 probe shown in Fig. 1, it can be approximated as a closed cylinder. The Effective Scan Volume (ESV), can be approximated as a second cylinder extending from the end of the probe. This representation of a bounding volume can be achieved by measuring a series of parameters of the probe such as length, radius, and radius of the ESV (equal to the radius of the detector film) as seen in Fig. 2. The depth of the ESV is determined by the Mean Free Path (MFP) of the radiation which is to be detected.

The top and face of the probe can be described as two hyperplanes separated by the length of the probe. Let a cylinder of radius, r, connect the 2 hyperplanes such that the intersection of these forms a convex hull, representing the probe, see Fig. 2 left. The ESV can be thought of as another cylinder with a smaller radius protruding from the front of the probe, see Fig. 2 right.

A hyperplane splits space in 2 which for 2 half-spaces, these can be represented in the form $B = \{\mathbf{x} \in \mathbb{R}^3 : \mathbf{n}^T(\mathbf{x} - \mathbf{x_0}) \leq 0\}$ for a given normal n and point on the hyperplane $\mathbf{x}_0$. For each $\mathbf{p}_i$, we can define a new point $\mathbf{s}_i = \mathbf{p}_i + d \cdot \mathbf{n}_i$, where d is equal to the desired stand-off distance of the probe and $\mathbf{n}_i$ is the normal at that point. This will act as the base point for the convex hull representing the probe and is the centre of the detector film. By defining 2 support vectors

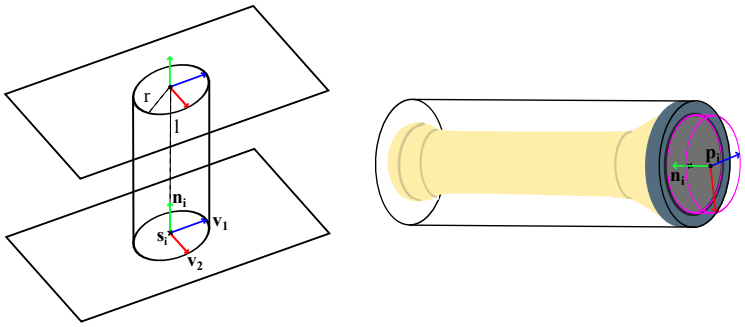

Fig. 2: Representation of two hyperplanes and cylinder forming a convex hull (left) and overlay of the convex hull representing the probe and ESV (purple) on top of the probe (right).

$\mathbf{v}_1 = \mathbf{n}_i \times [0,0,1]$, and $\mathbf{v}_2 = \mathbf{n}_i \times \mathbf{v}_1$, the set of half-spaces can be described by substituting the different values for normals and points into B to generate

$$\begin{aligned}
\mathcal{C}_{b_i} &= \{\mathbf{x} \in \mathbb{R}^3 : \mathbf{n}_i^T(\mathbf{x} - \mathbf{s}_i) \geq 0\} \\
\mathcal{C}_{t_i} &= \{\mathbf{x} \in \mathbb{R}^3 : \mathbf{n}_i^T(\mathbf{x} - (\mathbf{s}_i + l \cdot \mathbf{n}_i)) \leq 0\} \\
\mathcal{C}_{c_i} &= \{\mathbf{x} \in \mathbb{R}^3 : \mathbf{v}_1^T(\mathbf{x} - \mathbf{p}_i)(\mathbf{x} - \mathbf{p}_i)^T\mathbf{v}_1 + \mathbf{v}_2^T(\mathbf{x} - \mathbf{p}_i)(\mathbf{x} - \mathbf{p}_i)^T\mathbf{v}_2 - r^2 \leq 0\} \\
\mathcal{C}_{\text{probe}} &= \{\mathcal{C}_{t_i}, \mathcal{C}_{b_i}, \mathcal{C}_{c_i}\} \qquad (3)
\end{aligned}$$

where $\mathcal{C}_{\text{probe}}$ is the convex hull of the probe at each point $\mathbf{p}_i$, l is the length of the probe and r is the radius of the probe. The same approach can be taken for the modelling of the ESV

$$\begin{aligned}
\mathcal{C}_{b_i} &= \{\mathbf{x} \in \mathbb{R}^3 : \mathbf{n}_i^T(\mathbf{x} - \mathbf{s}_i) \leq 0\} \\
\mathcal{C}_{p_i} &= \{\mathbf{x} \in \mathbb{R}^3 : \mathbf{n}_i^T(\mathbf{x} - (\mathbf{p}_i - (a - d) \cdot \mathbf{n}_i)) \geq 0\} \\
\mathcal{C}_{c_i} &= \{\mathbf{x} \in \mathbb{R}^3 : \mathbf{v}_1^T(\mathbf{x} - \mathbf{p}_i)(\mathbf{x} - \mathbf{p}_i)^T\mathbf{v}_1 + \mathbf{v}_2^T(\mathbf{x} - \mathbf{p}_i)(\mathbf{x} - \mathbf{p}_i)^T\mathbf{v}_2 - r_s^2 \leq 0\} \\
\mathcal{C}_{\text{ESV}} &= \{\mathcal{C}_{p_i}, \mathcal{C}_{b_i}, \mathcal{C}_{c_i}\} \qquad (4)
\end{aligned}$$

with $\mathcal{C}_{\text{ESV}}$ being the convex hull representing the ESV at $\mathbf{p}_i$, a is the range over which the probe can reliably detect radiation determined by the MFP of radiation, and r_s is the radius of the scan zone.

2.3 Accessibility Assessment

The accessibility assessment determines the points within the set P representing the point cloud, which a given probe can both reach and effectively scan. For a point $\mathbf{p}_i$ to be valid, that is reachable without colliding, then none of the points within its neighbourhood can satisfy C_{probe}. If valid, then points it can effectively scan at $\mathbf{p}_i$ become any point within its neighbourhood which satisfies C_{ESV}. This

is visually represented in Fig. 4 This approach builds upon methods used within computer science for determining collisions between meshes or other objects [6]. The assessment considers collisions between the probe and the surface on which the object is placed, between the probe and the PC, as well as between the probe and other constraints modelled as planes.

It expands upon Discrete Collision detection (DCD) [15], which returns a boolean value to whether two objects have collided. This can be generalised to a function which assesses the intersections of a family of sets. Let I be an indexing set of the family of sets $\{A_i\}_{i\in I}$ then

$$f(A) = \begin{cases} 0, & \text{if } \bigcap_{i\in I} A_i = \emptyset \\ 1, & \text{otherwise} \end{cases} \tag{5}$$

that is to say, if the intersection of the family of sets is empty, it is classed as a disjoint set. If we define N_{r_i} using equation 1 with $r = l + 2 \cdot d$ and $A_i = \{N_{r_i}, \mathcal{C}_{\text{probe}}\}$, we can use the function to evaluate whether the probe collides with any neighbouring points. If the function returns 0, the sets do not intersect and the point is accessible, and if it returns 1, the point is inaccessible. Equation 5 can also be used to evaluate whether the probe will collide with the surface it's placed on, assumed to be a table, or whether the probe will collide with other constraints. Collisions with other constraints will not be considered. The table can be modelled as $\mathcal{C}_{\text{table}} = \{\mathbf{x} \in \mathbb{R}^3 : [0, 0, 1] \cdot \mathbf{x} \leq b\}$. While the intersection can be solved using linear programming, a more efficient method is posed in Section 2.4.

2.4 Collision with Table Surface

All objects to be scanned must be placed on a surface, whether that is the floor or a table, which adds a challenge in determining point accessibility. This issue can be simplified to evaluate if the vertices or the minimum point of $\mathcal{C}_{\text{probe}}$ intersects with $\mathcal{C}_{\text{table}}$. There are many approaches for solving this [6]. For convex hulls with vertices, detecting intersections with a half-space is straightforward. However, for $\mathcal{C}_{\text{probe}}$ without vertices, the minimal point of the convex hull is used to evaluate the collision with the flat surface. This can be posed as an optimisation problem, though it is computationally expensive.

Alternatively, leveraging the definition of $\mathcal{C}_{\text{probe}}$ allows reducing this to a constant time evaluation $\mathcal{O}(1)$. This is possible due to the definition of $\mathbf{v}_1$ and $\mathbf{v}_2$. Consider the intersection of the cylinder with the half-space $\mathcal{C}_{b_i}$ which forms a circle $Q \in \mathbb{R}^3$. If $\mathbf{n}_i$ has a positive z component, then the minimal point of the circle will also be the minimum point of $\mathcal{C}_{\text{probe}}$. Let Q be expressed as

$$Q = \mathbf{s}_i + r \cdot \cos t \cdot \mathbf{v}_1 + r \cdot \sin t \cdot \mathbf{v}_2, \quad t = [0, 2\pi) \tag{6}$$

where r is the radius of the cylinder. Due to the properties of a vector product, $\mathbf{v}_1$ will always be in the xy-plane and orthogonal to $\mathbf{n}_i$. As a result of the right-hand rule, the second vector product, $\mathbf{v}_2$, will always be collinear with and in the

direction of the minimum point. This minimum point will lie on the intersections of the circle Q with the line $\mathbf{r} = \mathbf{s}_i + t \cdot \mathbf{v_2}$. It can be shown that this intersection occurs at: $t = \frac{\pi}{2}, \frac{3\pi}{2}$, with the minimum point at $\frac{\pi}{2}$. Thus, it is only necessary to evaluate the equation 6 at $t = \frac{\pi}{2}$ to determine whether the probe intersects with $\mathcal{C}_{\text{table}}$. If $\mathbf{n}_i$ has a negative z component, then $\mathbf{s}_i$ is replaced by $\mathbf{s}_i + l \cdot \mathbf{n}_i$ in equation 6.

3 Results and Discussions

To demonstrate this approach several test models were selected. A flat box, a laptop in two positions: Laptop (1) - half closed, and Laptop (2) - open, along with a model of a torse [13] were used. PCs were generated from vertices taken from the .STL files.

The framework was implemented within MATLAB R2023a. The Octree library [17] was modified with additional functions to enable nearest neighbour searches, normal estimation and normal alignment using an MST. The framework can be described by Algorithm 1. The parameters used for the algorithm were taken from the radiation probe with radius 0.0335 m, length 0.222 m, stand-off distance 0.015 m, scan radius and range of 0.03 m and 0.02 m respectively. The points which represented the base of the objects were removed as these would not be captured during a 3D scan.

Algorithm 1 Accessibility Assessment

Require: r, l, d, r_s, a ▷ Radius, Length, Stand-off, Scan Radius, Scan Range
  function ACCESS(P,N_i)
    for $\forall \mathbf{p}_i \in P$ **do**
      $\mathbf{n}_i \leftarrow NormalEstimation(N_{p_i})$
      $\mathbf{v}_1 \leftarrow \mathbf{n}_i \times [0, 0, 1]$
      $\mathbf{v}_2 \leftarrow \mathbf{n}_i \times \mathbf{v}_1$
      if $!CollideWithTable(\mathbf{p}_i, \mathbf{v}_1, \mathbf{v}_2, r, l, d)$ **then**
        if $!f(\{N_{p_i}, \mathcal{C}_{\text{probe}}\})$ **then**
          $A_i \leftarrow True$ ▷ Set the accessibility of the point to True
          $DetermineScannedPoint(\mathbf{p}_i, \mathbf{v}_1, \mathbf{v}_2, r_s, a)$
        else
          $A_i \leftarrow False$ ▷ Set the accessibility of the point to False
        end if
      end if
    end for
  return A
  end function

Fig. 3 shows the output of the framework, the blue points represent poses within the PC where the probe will not collide with the surface if it approaches that point. The red points represent poses where the probe would collide with the table or PC. Consider Fig. 3c, the points which are considered inaccessible are those around the base and underside of the laptop, due to colliding with the half-space representing the table. Not as obvious are the points along the hinge

which are also flagged as inaccessible, this is expected due to the radius of the sensor and the small stand-off distance causing a collision between the probe and the screen/keyboard. Fig. 3a and Fig. 3d show successful coverage of the models with only the armpits and those along the base being inaccessible, The results of the framework showing accessible points and total coverage is presented in Table 1.

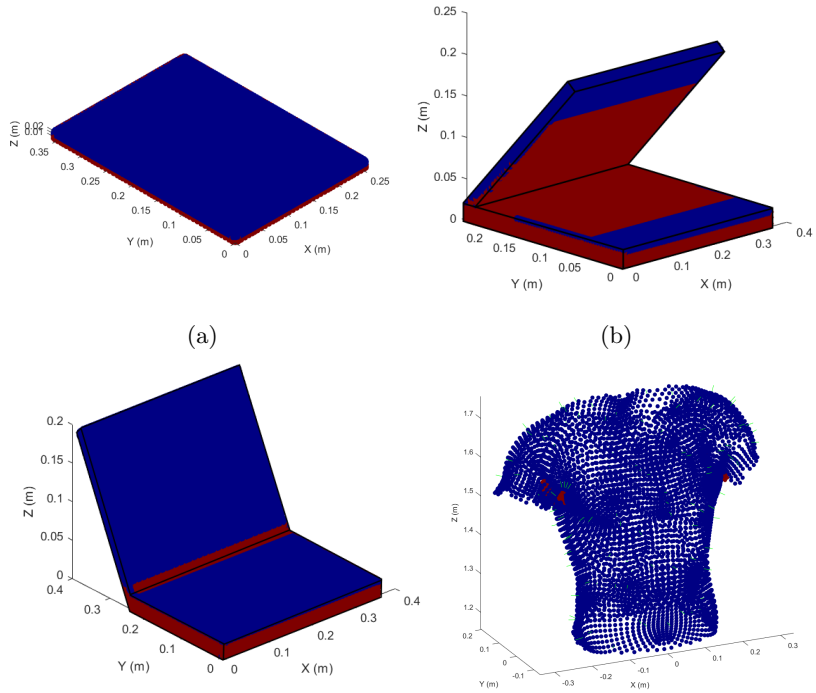

Fig. 3: Plots of the accessible points (blue) and inaccessible points (red) of both (a) flat box, (b) Laptop (1), (c) Laptop (2) and (d) Torso.

Fig. 3b has been used in Fig. 4 to illustrate several example cases, where the probe has been overlaid onto the PC to show how the framework simulates the probe and determines if a point will be accessible. Points around the base are inaccessible due to collisions with the table, and points at the innermost part of the screen are inaccessible as the probe collides with the points of the screen/keyboard. Those on the flat exterior surfaces are accessible and as such shown in blue.

This assessment does not consider the workspace of the manipulator or human conducting the assessment and is to identify areas of potential risk and points which can be used to plan safe trajectories. When assessing the performance of the approach, it is assumed that the octree, associated normals and clusters for each point have already been calculated via Section 2.1 with a min-

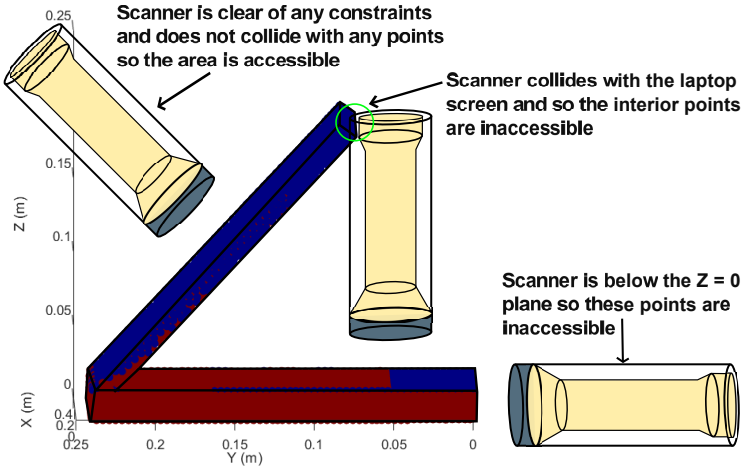

Fig. 4: Overlap of the probe onto the PC to illustrate the assessment process carried out in determining accessibility.

imum octant size of 0.005 m and maximum bin capacity of 8, which achieved a good compromise between the performance and resolution.

The performance of the algorithm can be assessed using several metrics such as execution time and time complexity, coverage, and visual inspection. From inspecting the generated plots, it is intuitive to see that the framework is performing as expected. However, there are some discrepancies in the normal estimation caused by the surface geometry. These points can be seen in Fig. 4 close to the hinge (e.g. $y = 0.2$ m, $z = 0.05$ m), this causes an uneven cut-off line instead of a straight cut-off. Although this inaccuracy is a limitation of the approach, it is representative of the process when using real-world data. Furthermore, being conservative in this way minimises the risk of collision.

Table 1: Results of the accessibility assessment for each generated point cloud.

Model	Points	Leafs	Accessible (%)	Coverage (%)	Assessment Time (s)
Flat Box	33932	7339	89.33	94.96	0.62
Laptop (1)	69653	18722	43.11	53.90	3.86
Laptop (2)	49646	17460	61.23	75.84	3.76
Torso	32424	5398	70.84	90.08	0.50

The evaluation of the execution time and time complexity, given the stated assumption, requires assessing the performance of Algorithm 1. Assuming all calculations and conditional statements execute in constant time, the dominant term in determining time complexity is the loop over each leaf octant of the octree. It is possible to conclude that this algorithm will execute in linear time $\mathcal{O}(n)$. In Table 1, accessible refers the the percentage of points within P which do not cause a collision with the probe if it approach that pose. However, some

points may not be directly accessible but fall within the ESV of the probe at another pose and therefore can be monitors, this is referred to as coverage.

The assessment achieving high accessibility and coverage over all models in reasonable execution time. With the flat box and torso achieving over 90% coverage, the results of the torso model are significant as the final intended system will perform radiological surveys over humans.

4 Conclusion and Future Work

The results presented in this paper demonstrate the effectiveness of the framework in distinguishing between accessible and inaccessible areas within point cloud data for radioactive contamination monitoring. By modelling the probe with geometric primitives and expanding on conventional discrete collision detection, the framework quickly assesses point clouds. Constraining the probe definition reduces the time complexity for detecting collisions between the probe and a surface to $\mathcal{O}(1)$. With minimal modification, this framework can be applied to other fields by adjusting parameters or defining new end-effector geometries.

This work could be included in existing manipulation frameworks and expanded to include non-convex end effector geometries that could be used outside of surface following, such as grasping. Future work will develop this framework to include various probe geometries in a dedicated library and use the output of the framework to investigate methods for discerning a near-optimal set of scan points to be used for constructing viable trajectories over the objects which will be used to perform surface contamination monitoring as part of a robotic radiological survey assistant.

Acknowledgements. This work is supported by funding from an Industrial Cooperative Awards in Science & Engineering (iCASE) by Nuclear Restoration Services Dounreay, the Nuclear Decommissioning Authority and EPSRC. AW acknowledges support from UK Research and Innovation via project EP/V026941/1.

References

1. Bryant, P.A.: The role of radiation protection societies in tackling the skills shortage and development of young professionals and researchers. Journal of Radiological Protection **41**(3), S79–S88 (Aug 2021). https://doi.org/10.1088/1361-6498/abf815
2. Graumann, C., Fuerst, B., Hennersperger, C., Bork, F., Navab, N.: Robotic ultrasound trajectory planning for volume of interest coverage. In: 2016 IEEE International Conference on Robotics and Automation (ICRA). IEEE (May 2016). https://doi.org/10.1109/icra.2016.7487201
3. Hackel, T., Wegner, J.D., Schindler, K.: Contour detection in unstructured 3d point clouds. In: 2016 IEEE Conference on Computer Vision and Pattern Recognition (CVPR). IEEE (Jun 2016). https://doi.org/10.1109/cvpr.2016.178
4. Hasegawa, T., Hashimoto, T., Hashimoto, M.: Radioactive contamination monitors. Fuji Jiho **36**, 373–379 (2004)

5. Hoppe, H., DeRose, T., Duchamp, T., McDonald, J., Stuetzle, W.: Surface reconstruction from unorganized points. In: Proceedings of the 19th annual conference on Computer graphics and interactive techniques. SIGGRAPH92, ACM (Jul 1992). https://doi.org/10.1145/133994.134011
6. Lin, M., Manocha, D.: Overview on Collision and Proximity Queries, p. 181–203. A K Peters/CRC Press (Jul 2008). https://doi.org/10.1201/b10636-12
7. Ly, K.T., Munks, M., Merkt, W., Havoutis, I.: Asymptotically optimized multi-surface coverage path planning for loco-manipulation in inspection and monitoring. In: 2023 IEEE 19th International Conference on Automation Science and Engineering (CASE). IEEE (Aug 2023). https://doi.org/10.1109/case56687.2023.10260625
8. Mauer, G.F., Kawa, C.: Accuracy Analysis of a Robotic Radionuclide Inspection and Mapping System for Surface Contamination. American Nuclear Society, United States (2008)
9. Management of Radiation Protection in Defence: part 2 guidance (jsp 392) (1 2023)
10. Monk, S.D., West, C., Bandala, M., Dixon, N., Montazeri, A., Taylor, C.J., Cheneler, D.: A low-cost and semi-autonomous robotic scanning system for characterising radiological waste. Robotics **10**(4), 119 (Nov 2021). https://doi.org/10.3390/robotics10040119
11. Nakhaeinia, D., Payeur, P., Chávez-Aragón, A., Cretu, A.M., Laganière, R., Macknojia, R.: Surface following with an rgb-d vision-guided robotic system for automated and rapid vehicle inspection. International Journal on Smart Sensing and Intelligent Systems **9**(2), 419–447 (Jan 2016). https://doi.org/10.21307/ijssis-2017-877
12. Nakhaeinia, D., Payeur, P., Laganiere, R.: A mode-switching motion control system for reactive interaction and surface following using industrial robots. IEEE/CAA Journal of Automatica Sinica **5**(3), 670–682 (May 2018). https://doi.org/10.1109/jas.2018.7511069
13. nixor: Male base mesh 3d model, bluehttps://free3d.com/3d-model/male-base-mesh-6682.html, [Accessed 24-06-2024]
14. Nuclear Skills Strategy Group: Nuclear Workforce Assessment (12 2023)
15. Pan, J., Chitta, S., Manocha, D.: Fcl: A general purpose library for collision and proximity queries. In: 2012 IEEE International Conference on Robotics and Automation. IEEE (May 2012). https://doi.org/10.1109/icra.2012.6225337
16. Pauly, M., Gross, M., Kobbelt, L.: Efficient simplification of point-sampled surfaces. In: IEEE Visualization, 2002. VIS 2002. VISUAL-02, IEEE (2002). https://doi.org/10.1109/visual.2002.1183771
17. Sven: octree - partitioning 3d points into spatial subvolumes
18. Thakur, V.M., Jain, A., Ashokkumar, P., Anilkumar, R., Sawant, P., Chaudhury, P., Chaudhari, L.M.: Design and development of a plastic scintillator based whole body β/γ contamination monitoring system. Nuclear Science and Techniques **32**(5) (May 2021). https://doi.org/10.1007/s41365-021-00883-1
19. Thermo Fisher Scientific: Non-Intelligent and Intelligent Scintillation Probes Instruction Manual (8 2006)
20. Von Haxthausen, F., Böttger, S., Wulff, D., Hagenah, J., García-Vázquez, V., Ipsen, S.: Medical robotics for ultrasound imaging: Current systems and future trends. Current Robotics Reports **2**(1), 55–71 (Feb 2021). https://doi.org/10.1007/s43154-020-00037-y
21. White, S.R., Megson-Smith, D.A., Zhang, K., Connor, D.T., Martin, P.G., Hutson, C., Herrmann, G., Dilworth, J., Scott, T.B.: Radiation mapping and laser profiling using a robotic manipulator. Frontiers in Robotics and AI **7** (Nov 2020). https://doi.org/10.3389/frobt.2020.499056